



1

2 **A nonstationary analysis for investigating the multiscale**  
3 **variability of extreme surges: case of the English Channel coasts**

4

5 Imen Turki<sup>1</sup>, Lisa Baulon<sup>1,2</sup>, Nicolas Massei<sup>1</sup>, Benoit Laignel<sup>1</sup>, Stéphane Costa<sup>3</sup>,  
6 Matthieu Fournier<sup>1</sup>, Olivier Maquaire<sup>3</sup>

7

8 <sup>1</sup> UMR CNRS 6143 Continental and Coastal Morphodynamics 'M2C' University of Rouen,  
9 76821 Mont-Saint-Aignan Cedex, France.

10 <sup>2</sup> French Geological Survey, 3 avenue Claude Guillemin, 45060 Orléans Cedex, France

11 <sup>3</sup>UMR CNRS 6554 GEOPEN

12 Corresponding author: Imen Turki ([imen.turki@univ-rouen.fr](mailto:imen.turki@univ-rouen.fr))

13

14 **Abstract**

15 This research examines the nonstationary dynamics of extreme surges along the English  
16 Channel coasts and seeks to make their connection to the climate patterns at different time-  
17 scales by the use of a detailed spectral analysis in order to gain insights on the physical  
18 mechanisms relating the global atmospheric circulation to the local-scale variability of the  
19 monthly extreme surges. The variability of extreme surges highlights different oscillatory  
20 components from the interannual (~1.5-years, ~2-4-years, ~5-8-years) to the interdecadal (~12-  
21 16-years) scales with mean explained variances of ~ 25 - 32 % and ~ 2 - 4 % of the total  
22 variability, respectively. Using the two hypotheses that the physical mechanisms of the  
23 atmospheric circulation change according to the timescales and their connection with the local  
24 variability improves the prediction of the extremes, we have demonstrated statistically  
25 significant correlations between ~1.5-years, ~2-4-years, and ~5-8-years and 12-16-years with  
26 the different climate oscillations of Sea-Level Pressure, Zonal Wind, North Atlantic Oscillation  
27 and Atlantic Multidecadal Oscillation, respectively.



28 Such physical links have been used to implement the parameters of the time-dependent GEV  
29 distribution models. The introduced climate information in the GEV parameters has  
30 considerably improved the prediction of the different time-scales of surges with an explained  
31 variance higher than 30%. This improvement exhibits their nonlinear relationship with the  
32 large-scale atmospheric circulation.

33 **Key-Words:** Coastal extreme surges, multiscale variability, climate oscillations, nonstationary  
34 GEV models

## 35 **1. Introduction**

36 Risks assessments has been recognized as an urgent task essential to take effective reduction  
37 of disasters and adaptation actions of climate change. The increase in coastal flood risk is  
38 generally driven by the extreme surges being the result of episodic water fluctuations due to  
39 waves and storm surges. High surges are considered as significant hazards for many low-lying  
40 coastal communities (e.g. Hanson et al., 2011; Nicholls et al., 2011) and are expected to be  
41 intensified with rising global mean sea level (Menendez and Woodworth, 2010).

42 Being an alarming problem for the coastal vulnerability, extreme events have gained the  
43 attention of the scientists who have reported the dynamics (e.g. Haigh et al., 2010; Idier et al.,  
44 2012; Masina and Lamberti, 2013; Tomasin and Pirazzoli, 2008; Turki et al., 2020) and the  
45 projections (e.g. vousedoukas et al., 2017) of extreme surges considering the stationary and the  
46 nonstationary contributions from tides, waves, sea-level-rise components (e.g. Brown et al.,



47 2010; Idier et al., 2017), and large-scale climate oscillations (e.g. Colberg et al., 2019; Turki et  
48 al., 2019; 2020).

49 Under the assumption of a stationary surges, the concepts of return level and return period  
50 provide critical information for infrastructure design, decision-making, and assessing the  
51 impacts of rare weather and climatic events (Rosbjerg and Madsen, 1998). However, the  
52 frequency of extremes has been changing and is likely to continue changing in the future (e.g.  
53 Milly et al., 2008). Therefore, concepts and models that can account for nonstationary analysis  
54 of climatic and hydrologic extremes are needed (e.g. Cooley, 2013; Salas and Obeysekera,  
55 2013; Parey et al., 2010).

56 Over the last decade, several studies adopted the nonstationary behaviour of extremes to  
57 estimate their evolution and their return-periods from rigorous models of Extreme Value  
58 Theory (EVT) by incorporating an information related to climate oscillations.

59 In this way, the recurrence of coastal extreme events over the Northern European continent and  
60 the persistence of high energetic conditions around the Atlantic have been associated with the  
61 deepening of Icelandic Low and the extension/reinforcement of the Azores High. Those facts  
62 can be interpreted, at quasi daily timescale, as the preferred excitation of a given atmospheric  
63 regime close to the positive phase of the North Atlantic Oscillation. The recent predominance



64 of this regime can be explained partly by the impact of the North Tropical Atlantic Ocean upon  
65 the midlatitude atmosphere and by the increase of greenhouse gas concentration induced by  
66 human activities.

67 Menendez and Woodworth (2010) have used a nonstationary extreme values analysis together  
68 with the NAO (North Atlantic Oscillation) and Arctic Oscillation (AO) indices for improving  
69 the estimation of monthly extreme sea-levels along the European coasts.

70 In the Northern Adriatic region, Masina et al. (2013) investigates changes in extreme sea levels  
71 applying a nonstationary approach to the monthly maxima and the climate oscillations of NAO  
72 and AO (Arctic Oscillation) indices. They have suggested that the increase in the extreme water  
73 levels since the 1990s is related to the changes in the wind regime and the intensification of  
74 Bora and Sirocco winds after the second half of the 20th century.

75 In the English Channel, the extreme sea levels have been addressed by several works (e.g.  
76 Haigh et al., 2010; Idier et al., 2012; Tomasin and Pirazzoli, 2008; Turki et al., 2015a; Turki et  
77 al., 2019) with the aim of investigating their dynamics at different timescales and their  
78 connections to the atmospheric circulation patterns.

79 Haigh et al. (2010) investigated the interannual and the interdecadal extreme surges in the  
80 English Channel and their strong relationship with the NAO index. Their results showed weak



81 negative correlations throughout the Channel and strong positive correlations at the boundary  
82 along the Southern North Sea. Using a numerical approach, Idier et al. (2012) studied the spatial  
83 evolution of some historical storms in the Atlantic Sea and their dependence on tides.  
84 Recently, Turki et al. (2019) have examined the multiscale variability of the sea-level changes  
85 in the Seine bay (NW France) in relation with the global climate oscillations from the SLP  
86 composites; they have demonstrated dipolar patterns of high-low pressures suggesting positive  
87 and negative anomalies at the interdecadal and the interannual scales respectively.  
88 Despite these important advances, no particular studies exist on sea-level dynamics and  
89 extreme events linked to the large-scale climate oscillations along the English Channel  
90 coastlines. The aforementioned works of Turki et al. (2015a, 2019) have focused on the  
91 multiscale sea-level variability along the French coasts related to the NAO and the Sea-Level  
92 Pressure (SLP) patterns; however, they have not addressed the regional behaviour of the  
93 extreme sea levels in relation with the global climate oscillations. Then, similar approaches  
94 have been used by Turki et al. (2020) to quantify the nonstationary behaviour of extreme surges  
95 and their relationship with the global atmospheric circulation at different timescales along the  
96 English Channel coasts (NW France). They have reported that the intermonthly and the



97 interannual variability of monthly extrema are statistically modelled by nonstationary GEV  
98 distribution using the physical mechanisms of the climate teleconnections.

99 The present contribution aims to investigate the multi-timescale dynamics of extreme surges  
100 along the English Channel coasts by the use of combining techniques of spectral analyses and  
101 probabilistic models. We hypothesize that different large-scale climate variables may be  
102 involved in explaining the occurrence of extreme surges, and that this dependence can be a  
103 function of timescale. The rationale behind this hypothesis is based on the following: (1) each  
104 timeseries of extreme surges should depend on different timescales; (2) each timescale should  
105 be related to a specific large-scale oscillation. Using this hypothesis, the linkages between the  
106 local extreme surges and the large-scale climate oscillations are deciphered with the aim to  
107 improve the extreme models using the most consistent large-scale oscillations as covariates.

108 The overall approach for testing our hypothesis can be described as follows, for a given extreme  
109 surge timeseries: i) identify the short to long timescale oscillations characterizing the local  
110 variability of the extreme surges; ii) explore the correlation between the local extreme surges  
111 and the selected large-scale variable from short to long timescales; iii) select the most  
112 appropriate large-scale variable as an explanatory parameter to be used as a covariate in  
113 nonstationary GEV models and estimate the extreme surges.



114 The paper is structured as follows. The used hydro-climatic data are presented in section 2,  
115 including local extreme surges and large-scale variables. Section 3 explains the methodological  
116 approach used. Finally, the sections 4 and 5 report the results related to the multiscale  
117 variability of extreme surges along the English Channel and their teleconnections with the  
118 large-scale climate oscillations required for their estimation by the use of GEV extreme models.  
119 The concluding remarks of these findings are addressed in section 6.

120  
121

## 2. Database description

122 The present research focuses on the dynamics of extreme surges along the English Channel  
123 coasts (French and the Britannic coasts); It has been conducted in the framework of some  
124 French research programs: RICOCHET (ANR program), RAIV COT (Normandy Region  
125 program) and the international project COTEST (CNES-TOSA program) related to the future  
126 mission Surface Water and Ocean Topography (SWOT).

127 The English Channel (Figure 1) is a shallow sea between Northern France and South England,  
128 connecting Atlantic Ocean to North Sea. Melting of retreating glaciers formed a megaflood in  
129 the southern North Sea and it geographically separated Britain from Europe and formed English  
130 Channel at the last Quaternary Period (Collier et al. 2015). English Channel has a complex  
131 sea floor due to its characteristics of formation. It is deep and wide on the western side,



132 narrower and shallower towards Strait of Dover. Largest width of the Channel is around 160  
133 km (Figure 1). The average depth of the channel is about 120 m. It gradually narrows eastward  
134 to a width of 35 km and depth of around 45 m in the Dover Strait. The east to west extent of  
135 the Channel is about 500 km. The overall width of shallow depths is wider in the French side  
136 of the channel. The extreme storm surges of this area are mostly occurred by low pressure  
137 systems from the Atlantic Ocean, propagating eastwards or storm surges propagating south  
138 from the North Sea (Law, 1975). The area is exposed to major storms from Atlantic side of the  
139 channel, having a maximum fetch of winds, from west to southeast then to northwest.

140 Three tide gauge sites along the French coasts have been used in the present study: (1) Dunkirk  
141 station which is a few kilometres away from Belgian borders, (2) Cherbourg station located on  
142 the Cotentin Peninsula and at the opening of the Atlantic Sea, (3) Brest station which is a  
143 sheltered bay located at the western extremity of metropolitan France and connected to the  
144 Atlantic Ocean.

145 Two tide gauge sites along the Britannic coasts have been used: (1) Dover station which is  
146 separated from Dunkirk by the North Sea and (2) Weymouth station symmetrically with  
147 respect to Cherbourg.





148 These stations provide time-series of hourly observations measurements until 2018. The French  
149 tide gauges are operated and maintained by the National French Center of Oceanographic Data  
150 (SHOM). The observations which correspond to the hydrographic zero level are referenced to  
151 zero tide gauge (Figure 1). The Britannic tide gauges are operated by the British  
152 Oceanographic Data Center; they provide hourly measurements until 2018.

153 Available data are summarized as the following: Brest (168 years between 1850 and 2018);  
154 Cherbourg and Dunkirk (54 years between 1964 and 2018); Dover (53 years between 1963 and  
155 2018); Weymouth (28 years between 1990 and 2018).

156 The hourly measurements suffer from some gaps of daily length distributed along the time-  
157 series. These gaps have been processed by the hybrid model for filling gaps developed by Turki  
158 et al. (2015b) by using the SLP as covariate in ARMA methods and the memory effects of the  
159 previous distribution of surges to estimate the missing values and fill the gaps. This model has  
160 been used in the recent works of Turki et al., (2019; 2020).

161 The large-scale atmospheric circulations are represented in the present analysis by four  
162 different climate indices which are considered as fundamental drivers in the Atlantic regions:  
163 the Atlantic Multidecadal Oscillation (AMO), the North Atlantic Oscillation (NAO), the Zonal  
164 Wind (ZW) component extracted at 850hPa, and the Sea-Level Pressure (SLP). Monthly time-



165 series of climate index have been provided by the NCEP-NCAR Reanalysis fields with the  
166 same period during which the sea-level observations were conducted.

### 167 **3. Methodological Approach**

#### 168 ***3.1 Wavelet spectral analysis***

169 The Continuous Wavelet Transform CWT is generally used for data analysis in hydrology,  
170 geophysics, and environmental sciences (Labat, 2005; Sang, 2013; Torrence and Compo,  
171 1998). This technique produces the timescale with the means of the Fourier transform contour  
172 diagram on which the time is indicated on the x-axis, the timescale (period,) on the y-axis, and  
173 the variance (power) on the z-axis.

174 Then, a wavelet multiresolution analysis has been used to decompose the signal of monthly  
175 extreme surges into different internal components corresponding to different timescales. This  
176 decomposition consists on applying a series of iterative filtering to the signal by the use of low-  
177 pass and high-pass filters able to produce the spectral components describing the total signal.

178 More details are presented in the recent works of Massei et al. (2017) and Turki et al., (2019).

179 In summary, the total signal has been separated into a relatively small number of wavelet  
180 components from high to low frequencies that altogether explains the variability of the signal;  
181 this will be illustrated later using the hourly measurements and the monthly maxima of surges.



182           **3. 2 Stationary and Nonstationary extreme value model**

183   Finally, and with the aim of addressing the nonstationary behaviour of extreme surges, the  
184   monthly maxima of the surges have been calculated and decomposed with the multiresolution  
185   analysis. Then, a nonstationary extreme value analysis based on the GEV distribution with  
186   time-dependent parameters (Coles, 2001) has been implemented to model the series of the  
187   monthly maxima surges. There are several GEV families which depend on the shape parameter,  
188   e.g. Weibull ( $\varepsilon < 0$ ), Gumbel ( $\varepsilon = 0$ ), and Fréchet ( $\varepsilon > 0$ ). The three parameters of the GEV (i.e.  
189   location  $\mu$ , scale  $\psi$ , shape  $\varepsilon$ ) are estimated by the maximum likelihood function.

190   The nonstationary effect was considered by incorporating the selected climate indices (NAO,  
191   AMO, ZW, and SLP) into the parametrization of the GEV models. Akaike Information  
192   Criterion (AIC) has been used to select the most appropriate probability function models. The  
193   methods of maximum likelihood were used for the estimation of the distribution's parameters.  
194   The approach used considers the location ( $\mu$ ), the scale ( $\psi$ ), and the shape ( $\varepsilon$ ) parameters with  
195   relevant covariates, which are described by a selected climate index:

196                                   
$$\mu(t) = \beta_{0,\mu} + \beta_{1,\mu}Y_1 + \dots + \beta_{n,\mu}Y_n \quad (1)$$

197                                   
$$\psi(t) = \beta_{0,\psi} + \beta_{1,\psi}Y_1 + \dots + \beta_{n,\psi}Y_n \quad (2)$$

198                                   
$$\varepsilon(t) = \beta_{0,\varepsilon} + \beta_{1,\varepsilon}Y_1 + \dots + \beta_{n,\varepsilon}Y_n \quad (3)$$



199 Where  $\beta_0, \beta_1, \dots, \beta_n$  are the coefficients, and  $Y_i$  is the covariate represented by the climate  
200 index. For each spectral component, only one climate index can be used to be introduced into  
201 the parameters  $\mu, \psi$ , and  $\varepsilon$  of the nonstationary GEV model (into one of them, into two of them  
202 or into the three parameters). With the aim of optimizing the best use of the climate index into  
203 the different GEV parameters, a series of sensitivity analyses were implemented for each time  
204 scale. The AIC measures the goodness of the fitting of the model (Akaike, 1973) to the relation  
205  $AIC = -2l + 2K$ ; where  $l$  is the log-likelihood value estimated for the fitted model, and  $K$  is the  
206 number of the model parameters. Higher ranked models should result from lower AIC scores.

#### 207 **4. Multi-timescale variability of extreme surges**

208 The variability of the monthly extreme surges along the English Channel coasts has been  
209 investigated using the continuous wavelet transform (CWT). In the spectrum of Figure 2, the  
210 colour scale represents an increasing power (variance) from red to blue and pink. The CWT  
211 diagrams highlight the existence of several scales for all sites with different ranges of  
212 frequencies: the interannual scales of  $\sim 1.5$ -yr,  $\sim 2$ -4-yr,  $\sim 5$ -8-yr and the interdecadal scale of  
213  $\sim 12$ -16-yr.  
214 The variability of surges is clearly dominated by the interannual frequencies ( $\sim 1.5$ -yr,  $\sim 2$ -4-  
215 yr,  $\sim 5$ -8-yr) explaining a mean variance between 32% and 25% of the total energy (Table 1).



216 In Dover and Weymouth, the low frequencies of  $\sim 2$ -4-yr are well-structured with a mean  
217 explained variance of 9.5% while it is of 7% for  $\sim 5$ -8-yr. These percentages decrease slightly  
218 for the French sites to 8% and 5%, respectively. At  $\sim 1.5$ -yr, the explained variance is higher  
219 than 16% and 13% respectively in Britannic and French coasts. The interdecadal frequency of  
220  $\sim 12$ -16-yr varies between 2% and 4% from the total signal. This frequency is not observed in  
221 the shortest timeseries of Weymouth (Table 1).

222 The interannual variability (time-scales higher than  $\sim 1$  year) seems to be highly represented in  
223 the monthly extrema CWT (Figure 2). It's not the case for the monthly mean surges (Figure  
224 3.a) where most power spectrum is concentrated on the annual cycle with an explained variance  
225 higher than 50%.

226 The time-dependent PDF of the monthly mean and maximum surges over a period of 10 years,  
227 for illustration purpose, is displayed in Figure 3.b. The  $\sim 1$ -yr component of monthly mean  
228 surges is largely manifested with a pronounced variation of the Gaussian curves in time; such  
229 variations take wavelengths of approximately  $\sim 2$ -yr and  $\sim 4$ -yr. This result exhibits that the  
230 interannual frequencies of  $\sim 2$ -yr and  $\sim 4$ -yr are modulated within the annual mode for the mean  
231 surges while they are implicitly quantified for the monthly maxima.



232 Results have been explored to investigate the nonstationary dynamics of surges at different  
233 timescales. We have applied the wavelet multiresolution decomposition of monthly extrema  
234 for each site. The process has resulted in the separation of several components with different  
235 time-scales. Only the wavelet components, with have been considered in this work. In this  
236 research, we are interested in the time-scales higher than 1 year, i.e. traduced by three  
237 interannual scales ( $\sim 1.5$ -yr,  $\sim 2$ -4-yr, and  $\sim 5$ -8-yr) and a interdecadal scale of  $\sim 12$ -16-yr. We  
238 focused only on the interannual and the interdecadal scales whose fluctuations correspond to  
239 the oscillation periods less than half the length of the record and exhibit a high-energy  
240 contribution on the variance of the total signal. The lowest frequency, corresponding to  $\sim 12$ -  
241 16-yr is easily calculated from the longest record of Brest.

242 Figure 4 shows a series of oscillatory components of surges from interannual to interdecadal  
243 scales, not easily quantified by a simple visual inspection of the signal. High similarities  
244 between the different sites have been highly observed for the interannual and the interdecadal  
245 scales of  $\sim 5$ -8-yr and  $\sim 12$ -16-yr while they are less pronounced at the small scales of  $\sim 1.5$ -yr.  
246 At this timescale, the differences in the extreme surges can be explained by local physical  
247 phenomena controlling their dynamics. Such processes are mainly induced by combining the  
248 effects of meteorological and oceanographic forces including changes in atmospheric pressures



249 and wind velocities in shallow water areas. Beyond  $\sim 1.5$ -yr, the variability of extreme surges  
250 at larger scales seems to be quite similar in terms of frequency and amplitude for the five sites.  
251 Such large variability reveals the physical effects of a global contribution related to climate  
252 oscillations. The extent of the large-scale oscillations is not strictly similar and changes  
253 according to the timescale variability since the dynamics of surges is not necessarily related to  
254 the same type of atmospheric circulation process. This relationship will be addressed later in  
255 the second part of this section.

256 Here, the multiscale variability of extremes has been investigated from the spectral components  
257 of surges along the English Channel coasts. This signal has been linearly extracted from the  
258 total sea level, provided by tide gauges, by the use of the classical harmonic analysis and thanks  
259 to the assumption that the water level is the sum of the mean sea level, tides, and surges. This  
260 assumption approximates the quantification of both components in the English Channel where  
261 the significant tide-surge interactions (Tomassin & Pirazzoli, 2008) and the effects of the sea-  
262 level rise on tides and surges are important (e.g. Idier et al., 2017). Neglecting this nonlinear  
263 interaction between the surges, tides, and the sea-level rise suggests some uncertainties in the  
264 estimation of the high frequencies of the spectral components between daily and monthly



265 scales, which is not the focus of the present work where the interannual and the interdecadal  
266 scales are investigated.

267 Similar interannual timescales have been observed along the French coasts of Dunkirk, Le  
268 Havre and Cherbourg in Turki et al., (2020) works where the intermonthly and the interannual  
269 variability of hourly surges has been investigated. They have demonstrated that the timescales  
270 smaller than  $\sim 1.5$ -yr are differently manifested between the different sites. These differences  
271 have been associated to the local variability of surges induced by combining the effects of  
272 meteorological and oceanographic forces including changes in atmospheric pressures and wind  
273 velocities in shallow water areas. As suggested in their researches, the mean explained variance  
274 of the interannual fluctuations ( $\sim 1.5$ -yr,  $\sim 2$ -4-yr, and  $\sim 5$ -8-yr) has been quantified in this  
275 work as 25% of the total surges along the French coasts. This value is higher than 32% in  
276 Weymouth and Dover where the explained variance of the interdecadal scales ( $\sim 12$ -16-yr) is  
277 also more important with 3.5% (compared to 2% for the French coasts). The interdecadal  
278 variability  $\sim 12$ -16-yr, provided by the spectral analysis of the extreme surges, have been  
279 evidenced by Turki et al., (2019) in the Seine bay (NW France). Strong physical relations have  
280 been exhibited between the interdecadal time of  $\sim 12$ -16-yr and the exceptional stormy events  
281 produced with surges higher than 10-year return period level. The connections between the





282 low-frequency components and the historical record of the exceptional events suggested that  
283 storms would occur differently according to a series of physical processes oscillating at multi-  
284 time-scales; these processes control their frequency and their intensity (Turki et al., 2019).  
285 The relationships linking storminess to the interannual and the interdecadal extreme surges  
286 have been reported by Turki et al., 2019; they have demonstrated that the behaviour of storms,  
287 in terms of their intensity and their frequency, is controlled by the large-scale variability of  
288 surges.  
289 Accordingly, the multiscale variability of extreme surges exhibits a nonstationary behaviour  
290 modulated by a non-linear interaction between the different interannual and the interdecadal  
291 timescales. Assessing the effect of the nonstationary behaviour at different timescales is  
292 important for improving the estimation of extreme values. For example, a time-dependent  
293 Generalized Extreme Value (GEV) distribution has been used by Turki et al. (2020) to model  
294 the nonstationary features contained in the sea level timeseries by introducing the climate  
295 oscillations into the implemented GEV parameters (location, scale and shape) in order to  
296 improve the fitting of extreme values.

297 **5. Large-scale climate North-Atlantic oscillations and their link to**  
298 **extreme surges in the English Channel**

299



300 In this part, a new hybrid approach combining the spectral analysis and the nonstationary GEV  
301 models has been used to investigate the connection between the multi-timescale variability of  
302 local surges and the large-scale climate North Atlantic oscillations.

### 303 ***5.1 To what extent would large-scale climate oscillations link extreme surges?***

304 The wavelet coherence (WC) diagrams between the monthly maxima of surges and the  
305 different climate indices of SLP, ZW, NAO, AMO, introduced previously as the main  
306 atmospheric circulation within the English Channel, are illustrated respectively in Figures 5, 6,  
307 7 and 8. Results provided by these diagrams highlight:

308 1. The connection between the climate oscillations and the extreme surges is manifested  
309 differently as a function of the timescale. From a visual inspection of the different  
310 spectra provided WC, the most significant correlations of extreme surges have been  
311 identified with SLP, ZW, NAO and AMO respectively at ~ 1.5-yr, ~ 2-4-yr, ~ 5-8-yr  
312 and ~ 12-16-yr.

313 2. Each timescale exhibits mainly strong links with its associated climate index (explained  
314 variance varying between 55% and 80%) and weak ones with other indices (explained  
315 variance varying between 15% and 5%). Table 2 summarizes the contribution of the



316 different climate oscillations in the different interannual and interdecadal timescales of  
317 extreme surges. Here, mean values between the different sites are presented.

318 For example, SLP diagrams reveal significant relationships with  $\sim 1.5$ -yr surges (well-  
319 structured forms with high concentration of pink-blue colours in Figure 5); limited  
320 correlations, locally positioned in time, have been observed at  $\sim 2$ -4-yr and  $\sim 5$ -8-yr scales.

321 ZW shows strong correlations with interannual surges at  $\sim 2$ -4-yr (blue to pink colour at  
322 this scale; Figure 6) and others correlations at smaller and larger timescales of  $\sim 1.5$ -yr and  
323  $\sim 5$ -8-yr, respectively. Similarly, NAO presents high links with  $\sim 5$ -8-yr surges and small  
324 relations with  $\sim 2$ -4-yr and  $\sim 1.5$ -yr (Figure 7).

325 The  $\sim 1.5$ -yr scale highlights high correlations with SLP with an explained variance of 75%;  
326 25% of this scale should be explained by the influence of other climate oscillations (basically  
327 ZW and NAO with a mean explained variance of 10% and 6%, respectively; Table 2) and the  
328 combining effects of local driven forcing induced by winds and waves.

329 65% of  $\sim 2$ -4-yr scale is correlated with ZW while 5% and 12% is explained by the effect of  
330 NAO and SLP, respectively. The effects of NAO on the  $\sim 5$ -8-yr vary between 55% and 65%;  
331 minor influence at this scale has been observed with SLP and ZW explaining a mean variance



332 of 13%. The interannual scales of surges are slightly influenced by AMO oscillations with low  
333 values of variance lower than 1% (Table 2).

334 At interdecadal scales of ~ 12-16-yr, the extreme surges are mainly controlled by the AMO  
335 oscillations with a mean explained variance of 80% while the effects of NAO is limited to 10%.

336 Figure 9 displays the spectral components of the four climate oscillations, provided by a multi-

337 resolution analysis, together with the spectral components extracted from the extreme surges

338 (Figure 4) with the aim to quantify the different connections between both variables at the

339 interannual and the interdecadal timescales. For each spectral component of surges, a series of

340 Monte Carlo simulations has been carried out to identify the most statistically significant

341 correlation with the climate index of the respective timescale. The best correlation of each

342 surge component (i.e. ~ 1.5-yr, ~ 2-4-yr, ~ 5-8-yr and ~ 12-16-yr) with the suitable climate

343 index time scale ( i.e. SLP, ZW, NAO and AMO) is illustrated in Figure 9.

344 The interannual and the interdecadal variability of extreme surges and their multiscale

345 connection with the climate oscillations highlight the nonlinear relationship between large- and

346 local- scales.

347 Therefore, the interannual and the interdecadal extreme surges have proven to be strongly

348 related to different composites of oscillating atmospheric patterns. Such composites seem to be



349 not necessarily similar for the different timescales. The use of a multiresolution approach to  
350 investigate the dynamics of the extreme surges into the downscaling studies proves to be useful  
351 for assessing the nonstationary dynamics of the local extreme surges and their nonlinear  
352 interactions with the large-scale physical mechanisms related to climate oscillations.

353 Investigating the complex relationships between the climate oscillations and the multi-  
354 timescale surges has exhibited a multimodel climate ensemble that should be used to better  
355 understand this complexity.

356 The interannual connections between the local hydrodynamics and the climate variability have  
357 been investigated in numerous previous works focused on the atmospheric circulation with  
358 different related mechanisms (e.g., Feliks et al., 2011; Lopez-Parages et al. 2012; Zampieri et  
359 al., 2017). As demonstrated by the recent works of Turki et al. (2019, 2020), the effects of SLP  
360 oscillations on the  $\sim 1.5$ -yr variability of extreme surges are described by dipolar patterns of  
361 high-low pressures with a series of anomalies which are probably induced by some physical  
362 mechanisms linked to the North-Atlantic and ocean/atmospheric circulation oscillating at the  
363 same timescale.



364 The SLP fields combined with the baroclinic instability of wind stress have been related to the  
365 Gulf Stream path as given by NCEP reanalysis (Frankignoul et al., 2011); the dominant signal  
366 is a northward (southward) displacement of the Gulf Stream when the NAO reaches positive  
367 (negative) extrema. Daily mean SLP fields have been used by Zampieri et al. (2017) to analyse  
368 the influence of the Atlantic sea temperature variability on the day-by-day sequence of large-  
369 scale atmospheric circulation patterns over the Euro-Atlantic region. They have associated the  
370 significant changes in certain weather regime frequencies to the phase shifts of the AMO. For  
371 hydrological applications, several works have investigated the multiscale relationships between  
372 the local hydrological changes and the climate variability. Lavers et al. (2010) associated the  
373 7.2-yr timescales to SLP patterns which are not exactly reminiscent of the NAO and define  
374 centers of action which are shifted to the North.

375 Regarding the ZW (u850), results have shown its correlation with the interannual scales of ~2-  
376 4-yr extreme surges as suggested also in the recent findings of Turki et al. (2020). Its influence  
377 has been proven also at smaller (~1.5-yr) and larger scales (5-8-yr). Additionally to extreme  
378 surges, the interaction between the ZW and the temperature at different timescales has been  
379 highlighted in some previous researches (e.g., Andrade et al., 2012; Seager et al. 2003;  
380 Woodworth et al., 2007). Along UK and Northern English Channel coasts, Changes in trends



381 of extreme waters and storm surges have been explained by variations of energy pressure and  
382 ZW variability additional to thermosteric fluctuations linked to NAO (Woodworth et al., 2007).  
383 Andrade et al. (2012) have used the component of ZW at 850 hPa to investigate the positive  
384 and the negative phases of the extreme temperatures in Europe and their occurrence in relation  
385 with the large-scale atmospheric circulation. They suggested that both phases are commonly  
386 connected to strong large-scale changes in zonal and meridional transports of heat and  
387 moisture, resulting in changes in the temperature patterns over western and central Europe  
388 (Corte-Real et al., 1995; Trigo et al., 2002). The physical connections between ZW and the  
389 extreme events from 11 Global Climate Model runs have been demonstrated by the studies  
390 from Mizuta (2012) and Zappa et al (2013); they have suggested the complex relationship  
391 between the climate oscillation and the jet stream activity. They have found a slight increase  
392 in the frequency and strength of the storms over the central Europe and decreases in the number  
393 of the storms over the Norwegian and Mediterranean seas.  
394 The NAO is considered as an influencing climate driver for the large-scale atmospheric  
395 circulation, as suggested by other researches (e.g. Marcos et al., 2009; Philips et al., 2013).  
396 The existence of long-term oscillations originating from large-scale climate variability and thus  
397 controlling the interannual extreme surges has been highlighted from investigating the low



398 frequencies of the sea levels along the English Channel. This is in agreements with the results  
399 recently demonstrated by Turki et al. (2020) and the present finding exhibiting the strong links  
400 between NAO oscillations and the ~ 5-8-yr extreme surges along the English Channel coasts.  
401 The physical mechanisms related to the effects of the continuous changes in NAO patterns on  
402 the sea-level variability have been addressed in several studies (e.g., Marcos et al., 2005;  
403 Tsimplis et al., 1994). At the interannual scales, the key role of NAO on the sea-level variability  
404 has been explained by some previous works: Philips et al. (2013) investigated the influence of  
405 the NAO on the mean and the maximum extreme sea levels in the Bristol Channel/Severn  
406 Estuary. They have demonstrated that when high NAO winters increase in the positive phase,  
407 wind speeds also escalate while increasing the negative NAO winters results in low wind  
408 speeds. Then, the correlation between the low/high extreme surges and the NAO in the Atlantic  
409 has demonstrated a proportionality between NAO values and the augmentation in the winter  
410 storms. Feliks et al. (2011) defined significant oscillatory timescales of ~ 2.8-yr, ~ 4.2-yr, and  
411 ~ 5.8-yr from both observed NAO index and NAO atmospheric marine boundary layer  
412 simulations forced with SST; they have suggested that the atmospheric oscillatory modes  
413 should be induced by the Gulf Stream oceanic front.





414 Strong correlations between the monthly extreme surges and the AMO oscillations have been  
415 identified at the timescale of 12-16-yr (Figure 8 and Figure 9; in particular for Brest). Since the  
416 period of 1990's, the AMO and the extreme surges oscillate in opposition of phase. This shift  
417 should be explained by a substantial change in European climate manifested by cold wet and  
418 hot dry summers in the northern and the southern Europe, respectively; as discussed by Sutton  
419 and Dong (2012). They have demonstrated that the patterns, identified from the European  
420 climate change around 1990's, are synchronised with changes related to the North Atlantic  
421 Ocean.

422 Other weak links with the AMO have been identified at the interannual timescales of ~5-8-yr.  
423 along the studied sites. In agreement of previous works (e.g., Enfield et al., 2001; Zampieri et  
424 al., 2013; 2017), the effects of the AMO oscillations are mainly manifested at the interannual  
425 timescales to control the variability of hydrological (e.g. rainfall) and oceanographic (e.g.  
426 surges) variables. Generally, the climate oscillations of AMO are associated to the SST  
427 variability with a time cyclicity of about 65-70-years (e.g. Delworth and Mann, 2000; Enfield  
428 et al., 2001). During the warming periods of the 1990's, the AMO shifts from the negative to  
429 the positive phases in the Northern Hemisphere corresponding to cold and warm periods (e.g.  
430 Gastineau et al., 2012; Zhang et al., 2013). This shift can be responsible on changes in the  
431 hydrodynamic conditions (e.g. Zampieri et al., 2013).

432 The influence of the AMO oceanic low frequencies in the modulation of the mechanisms of  
433 the atmospheric teleconnections at the interannual timescales has been investigated in many  
434 previous works (e.g Enfield et al. 2001). At decadal timescales, the existing relationships  
435 between the winter NAO and the AMO variability is more complex (e.g. Peings and  
436 Magnusdottir, 2014).



437 The effects of the AMO-driven climate variability on the seasonal weather patterns have been  
438 investigated by Zampieri et al. (2017) in Europe and the Mediterranean. They have  
439 demonstrated significant changes in the frequencies of weather regimes involved by the AMO  
440 shifts which are in phase with seasonal surface pressure and temperature anomalies. Such  
441 regimes, produced in Spring and Summer periods, are differently manifested in Europe with  
442 anomalous cold conditions over Western Europe (Cassou et al., 2005; Zampieri et al., 2017).

443 In summary, four atmospheric oscillations have proven to be significantly linked to the  
444 interannual and interdecadal variability of extreme surges. This physical link varies according  
445 to the timescale exhibiting a nonlinear interaction of the same oscillations with other scales.

446 Such nonlinear behavior depends on the dynamics of the different sequences of the atmospheric  
447 and water vapour transport patterns during the month prior to the sea-level observations (e.g.  
448 Lavers et al., 2015). As suggested by Turki et al. (2020), the atmospheric circulation acts as a  
449 regulator controlling the multiscale variability of extreme surges with a nonlinear connection  
450 between the large-scale atmospheric circulation and the local scale hydrodynamics. This multi-  
451 timescale dependence between the local extreme dynamics and the internal modes of climate  
452 oscillations is still under debate. Understanding these physical links, even their complexities,  
453 are useful to improve the estimation of the extreme values in coastal environments; which is  
454 the objective of the next part.

## 455 *5.2 Nonstationary modelling of extreme surges*



456 In this part, stationary and nonstationary extreme value analyses based on GEV distribution  
457 with time-dependent parameters (Coles, 2001) have been implemented to model separately the  
458 different spectral components of extreme surges. Four GEV stationary (GEV0) and  
459 nonstationary (GEV1, GEV2 and GEV3) models have been applied to each timescale and each  
460 site. The GEV distribution uses the maximum likelihood method by parametrizing the location,  
461 scale, and shape of the model. We have used the ‘trust region reflective algorithm’ for  
462 maximizing the log-likelihood function (Coleman and Li, 1996).

463 The connections between the climate oscillations and the monthly maxima at the different  
464 timescales have been explored for the implementation of the nonstationary GEV models  
465 (Figure 9). For each spectral component, associated with its best climate index describing the  
466 internal oscillations of surges, three nonstationary models have been used by introducing the  
467 climate information as a covariable into: (1) the location parameter (GEV1); (2) both location  
468 and scale parameters (GEV2); (3) all location, scale and shape parameters (GEV3). The  
469 structure of the most appropriate nonstationary GEV distribution has been selected by choosing  
470 the most adequate parametrization that minimizes the Akaike information criterion (Akaike,  
471 1974). The goodness of fit for each model has been checked through the visual inspection of  
472 the quantile-quantile (Q-Q) plots (Figure 10); these plots compare the empirical quantiles



473 against the quantiles of the fitted model. Any substantial departure from the diagonal indicates  
474 inadequacy of the GEV model.

475 At the interannual scales and for all sites, results provided by the nonstationary GEV1-3 reveal  
476 a better performance (the lowest values of AIC) of extreme estimation compared to the  
477 stationary models of GEV0 and give the most appropriate distributions by the use of the climate  
478 large-scale covariates for specific oscillating components of extreme surges. Nevertheless, this  
479 improvement from the stationary to the nonstationary models has not been clearly observed for  
480 the interdecadal scales where the extreme estimation, provided by the different GEV models,  
481 is very similar (Table 3). The lowest values of AIC have been shown by GEV3 for ~1.5-yr,  
482 GEV2 for ~2-4-yr and GEV1 for ~5-8-yr (Table 4). The Q-Q plots for the all timescales of all  
483 timescales of the monthly maxima in Brest are illustrated in Figure 10; they confirm the  
484 suitability of the selected models.

485 Accordingly, the nonstationary GEV models have exhibited high improvements at the  
486 interannual scales where the AIC scores have significantly decreased by introducing the  
487 climate information into the parametrization of the model. Such consideration varies as a  
488 function of the spectral components, it concerns all parameters for the smallest scale of ~1.5-



489 yr, both location and scale parameters for ~2-4-yr and only the location parameter for largest

490 scale of ~5-8-yr.

491 Then, the large-scale oscillations introduced for the implementation of GEV parameters depend

492 on the time scale for all sites exhibiting a high nonstationary behaviour of the small interannual

493 scales (~1.5-yr) which decreases at the large interannual scales (~5-8-yr) and get non-

494 significant at the interdecadal scales (~ 12-16-yr).

495 The use of the time-varying GEV parameters at the interannual scales (~ 1.5-yr and ~ 2-4-yr)

496 exhibits the relationship between the mode and the standard deviation of the GEV distributions

497 associated with the location and the scale parameters, respectively.

498 The different implications of both parameters for estimating the interannual extreme surges

499 reveal cyclic variations and timescale modulations related to the large-scale climate

500 oscillations. As documented in the previous works (e.g., Menendez et al., 2009; Masina and

501 Lamberti., 2013), the location and the scale parameters used for improving the nonstationary

502 estimation of the extreme water levels highlight a series of annual and semi-annual evolutions.

503 They have reported that the seasonal cycles of the location parameter are related to two maxima

504 of water levels, in early March and September produced during equinoctial spring tides, while

505 the seasonal cycles of the scale parameter are associated to an increase of storms during wintry



506 episodes. Here, we focus on the stochastic signal of surges at scales larger than one year. The  
507 SLP and the ZW frequencies, introduced in the location and the scale parameters of  
508 nonstationary GEV models, determine an enhancement in the prediction of the interannual  
509 scales.

510 The shape parameter, implied for the estimation of the ~1.5-yr extreme surges, derives from its  
511 determination of the upper tail distribution behaviour. The time-varying shape parameter uses  
512 the ~1.5-yr SLP exhibiting altering negative and positive oscillations.

513 Despite its critical significance, the shape GEV parameter has revealed its relationships with  
514 basin attributes in hydrological applications and regional flood frequency analysis (e.g., Tyralis  
515 et al., 2019). The dependence of the shape parameter on the climate oscillations has been  
516 demonstrated in several extreme frameworks related to hydrological and oceanographic  
517 applications (e.g., Menendez et al., 2009; Masina et al., 2013; Turki et al., 2020). Regarding  
518 the stationarity of the surge timescale, the ~12-16-yr window sliding matches have been  
519 quantified in the previous part exhibiting a substantial cyclic variability consequence of an  
520 altering periods of positive and negative correlations. The modelling of the interdecadal  
521 extreme surges involves a stationary behavior of the ~12-16-yr.

522 A stationary trend of the SST anomalies associated with the AMO over the Euro-Atlantic  
523 region has been reported by Zampieri et al. (2017). They have showed that the low-frequency  
524 variability of the European Climate is influenced by the AMO shift induced by the phase  
525 opposition between the negative NAO distribution and the Atlantic patterns.



526 The return levels of the multiscale extreme surges, provided by the best GEV models (Table  
527 3), have been simulated. The example of Brest is illustrated in Figure 10.b for the interannual  
528 (nonstationary GEV models) and the interdecadal (GEV stationary model) scales. The 95%  
529 confidence interval is also plotted in this graph through a dashed black line. Accordingly, the  
530 use of GEV distribution with time-dependent parameters for each timescale should improve  
531 the evaluation of the return values and reduce the uncertainty of the quantile estimates.

532 The present approach does not resolve the nonlinear interactions between the large-scale  
533 climate oscillations and their influence on the estimation of the local extreme surges. Instead,  
534 each timescale has been simulated separately with the nonstationary GEV models and  
535 expressed as a function of the most suitable climate index improving its fitting. The estimation  
536 of the total signal of surges should be determined by combining the developed models used for  
537 the different timescales. Such combination requires integrating techniques

## 538 **6. Summary and Concluding remarks**

539 The dynamics of extreme surges together with the large-scale climate oscillations have been  
540 investigated by the use of hybrid methodological approach combining spectral analyses and  
541 nonstationary GEV models. Results have demonstrated that the interannual variability of  
542 extreme surges ( $\sim 1.5$ -yr,  $\sim 2$ -4-yr and 5-8-yr) is around 25% for the French coasts and higher



543 than 32% for the Britannic coasts; the interdecadal variability (~12-16-yr) varies between 2%  
544 and 4%. The fluctuations of extreme surges at ~1.5-yr are differently manifested between the  
545 different sites of the English Channel exhibiting a local variability of surges induced by the  
546 effects of meteorological and oceanographic forces including changes in atmospheric pressures  
547 and wind velocities in shallow water areas. Similar fluctuations have been observed at larger  
548 scales of the interannual and the interdecadal variability. Changes in extreme surges (~1.5-yr,  
549 ~2-4-yr, ~5-8-yr and ~12-16-yr) have been proven to be significantly linked to atmospheric  
550 oscillations (SLP, ZW, NAO and AMO, respectively) according to the timescale with a  
551 nonlinear interaction between different oscillations at the same scale. This exhibits the complex  
552 physical mechanisms of the global atmospheric circulation acting as a regulator and controlling  
553 the local variability of extreme surges at different timescales. The connections between the  
554 multiscale extreme surges and the internal modes of climate oscillations have been explored to  
555 improve the estimation of extreme values by the use of nonstationary GEV models. The  
556 simulated extreme surges have highlighted that introducing the climate oscillations for the  
557 implementation of GEV parameters depends on the timescale for all sites; a high nonstationary  
558 behaviour of the small interannual scales (~1.5-yr) decreases at the larger scales (~5-8-yr) and  
559 seems to be non-significant at the interdecadal scales (~ 12-16-yr).





560 The conclusion of this research suggests that the physical mechanisms driven by the  
561 atmospheric circulation, including the Gulf Stream gradients, play a key role in coastal extreme  
562 surges. Establishing a strong connection of the large-scale climate oscillations with extreme  
563 surges and flooding risks improve the estimation of the return levels.

564 This finding can represent a step forward in (1) the physical relation of downscaling from the  
565 global climate patterns to the local extreme surges; (2) inferring the future projections of sea  
566 level change and extreme events.

## 567 **Acknowledgments**

568 The research programs ‘RICOCHET’, ‘RAIV COT’, ‘REVE COT’ and CNES-TOSCA  
569 ‘COTEST’ are acknowledged for funding this research. elated to the future mission of Surface  
570 Water and Ocean Topography (SWOT). We also acknowledge the National Navy  
571 Hydrographic Service (SHOM), in particular Nicolas Pouvreau and Gael André, the British  
572 Oceanographic Data Center and the National Center for Environmental Prediction for  
573 providing sea level and atmospheric data.

## 574 **References**



- 575 Akaike, H.: Information theory as an extension of the maximum likelihood principle. In:  
576 Petrov, B. N., and Csaki, F. (Eds.), Second International Symposium on Information Theory,  
577 Akademiai Kiado, Budapest, pp. 267–281, 1974.
- 578 Andrade, C., Leite, S. M., and Santos, J. A.: Temperature extremes in Europe: overview of  
579 their driving atmospheric patterns. *Natural Hazards Earth System Sciences*, 12, 1671–1691,  
580 <https://doi.org/10.5194/nhess-12-1671-2012>, 2012.
- 581 Bell, R., G., and Goring, D., G.: Seasonal Variability of Sea Level and Sea-surface Temperature  
582 on the North-east Coast of New Zealand. *Estuarine, Coastal and Shelf Science*, 46 (2), 307-  
583 319, <https://doi.org/10.1006/ecss.1997.0286>, 1998.
- 584 Bessoumoulin, P.: Les tempêtes en France. *Annales des Mines*. 9-14, 2002.
- 585 Brown, J., Souza, A., and Wolf, J.: Surge modelling in the eastern Irish Sea: Present and future  
586 storm impact, *Ocean Dynamics* 60(2), 227–236, doi:10.1007/s10236-009-0248-8, 2010.
- 587 Carter, D. J. T., and Challenor, P.G.: Estimating return values of environmental parameters.  
588 *Quarterly Journal of the Royal Meteorological Society*, 107, 259-266, 1981.
- 589 Caspar, R., Costa, S., Lebreton, P., and Letortu, P.: Storm surges of the 10-11 march 2008 on  
590 the Albâtre Coast (Haute-Normandy, France): meteo-marine determination. *NOROIS*, p.115-  
591 132, <https://doi.org/10.4000/norois.3273>, 2010
- 592
- 593 Cassou, C., Terray, L., and Phillips, A.S.: Tropical Atlantic influence on European heat waves.  
594 *Journal of Climate*, 18, 2805–2810, 2005.
- 595 Ciasto, L.M., and Thompson, D.W.J.: North Atlantic Atmosphere-Ocean Interaction on  
596 Intraseasonal Time Scales. *Journal of Climate*, 17, 1617 – 1621, 2004.
- 597 ey, D. et al.: “Bayesian spatial modelling of extreme precipitation return levels” . *Journal of*  
598 *American Statistical Association*, 102: 824-840, 2007.



- 599 Colberg, F., McInnes, K.L., Grady, J., and Hoeke, R.: Atmospheric circulation changes and  
600 their impact on extreme sea levels around Australia. *Natural Hazards Earth System Sciences*,  
601 19, 1067–1086. <https://doi.org/10.5194/nhess-19-1067-2019>, 2019.
- 602 Coleman, T. F., Li, Y.: An interior trust region approach for nonlinear minimization subject  
603 to bounds. *SIAM Journal on Optimization*, 6(2), 418–445. doi:10.1137/0806023, 1996.
- 604 Coles, S.: *An Introduction to Statistical Modelling of Extreme Values*, Springer, London, U.  
605 K., 2001.
- 606 Collier, J.S., Oggioni, F., Gupta, S., García-Moreno, D., Trentesaux, A., and De Batist, M.:  
607 Streamlined Islands and the English Channel Megaflood Hypothesis. *Global and Planetary*  
608 *Change*, 135, 190–206. <https://doi.org/10.1016/j.gloplacha.2015.11.004>, 2015.
- 609 Corte-Real, J., Zhang, Z., and Wang, X.: Large-scale circulation regimes and surface climatic  
610 anomalies over the Mediterranean. *International Journal of Climatology*, 15, 1135–1150,  
611 <https://doi.org/10.1002/joc.3370151006>, 1995.
- 612 Enfield, D.B., Mesta-Nunez, A.M., and Trimble, P.J.: The Atlantic multidecadal oscillation  
613 and its relation to rainfall and river flows in the continental U.S. *Geophysical Research Letters*,  
614 28 (10), 2077–2080, 2001.
- 615 Delworth, T.L., and Mann, M.E.: Observed and simulated multidecadal variability in the  
616 Northern Atlantic. *Climate Dynamics*. 16, 661–676, 2002.
- 617 Feliks, Y., Ghil, M., and Robertson, A.W.: The atmospheric circulation over the North Atlantic  
618 as induced by the SST field. *Journal of Climate*, 4 (2), 522–542,  
619 <http://dx.doi.org/10.1175/2010JCLI3859.1>, 2001.
- 620 Frankignoul, C., N. Sennechael, Y., Kwon, O., and Alexander, M.A.: Influence of the  
621 Meridional Shifts of the Kuroshio and the Oyashio Extensions on the Atmospheric Circulation.  
622 *Journal of Climate*, 24, 762 – 777, <https://doi.org/10.1175/2010JCLI3731.1>, 2011.



- 623 Gastineau, G., D'Andrea, F., and Frankignoul, C.: Atmospheric response to the North Atlantic  
624 Ocean variability on seasonal to decadal time scales. *Climate Dynamics*, 2012.
- 625 Gupta, S., Collier, J.S., Andy, P.F., and Potter, G.: Catastrophic Flooding Origin of Shelf  
626 Valley Systems in the English Channel. *Nature*, 448 (7151): 342–45.  
627 <https://doi.org/10.1038/nature06018>, 2007.
- 628 Haigh, I., Nicolls, R., and Wells, N.: Assessing changes in extreme sea levels: Application to  
629 the English Channel 1900-2006. *Continental Shelf Research*, 30, 1042-1055.  
630 <https://doi.org/10.1016/j.csr.2010.02.002>, 2010.
- 631 Haigh, I., Nicolls, R., and Wells, N.: Mean sea level trends around the English Channel over  
632 the 20<sup>th</sup> century and their wider context. *Continental Shelf Research*, 29, 2083-2098.  
633 <https://doi.org/10.1016/j.csr.2009.07.013>, 2009.
- 634 Hanson, S., Nicholls, R., Ranger, N., Hallegatte, S., Dorfee-Morlot, J., Herweijer, C., and  
635 Chateau, J.: A global ranking of port cities with high exposure to climate extremes. *Climate*  
636 *Change*, 104(1), 89-111, [10.1007/s10584-010-9977-4](https://doi.org/10.1007/s10584-010-9977-4), 2011.
- 637 Idier, D., Dumas, F., and Muller, H.: Tide-surge interaction in the English Channel. *Natural*  
638 *Hazards Earth System Sciences*, 12, 3709–3718. doi:10.5194/nhess-12-3709-2012, 2012.
- 639 Idier, D., Paris, F., Le Cozannet, G., Boulahya, F., and Dumas, F.: Sea-level rise impacts on  
640 the tides of the European Shelf, *Continental Shelf Research*, 56-71.  
641 <https://doi.org/10.1016/j.csr.2017.01.007>, 2017.
- 642
- 643 Labat, D.: Recent advances in wavelet analyses: Part 1. A review of concepts. *Journal of*  
644 *Hydrology*, 314 (1–4), 275–288. <http://dx.doi.org/10.1016/j.jhydrol.2005.04.003>, 2005.
- 645 Lavers, D.A., Hannah, D.M., and Bradley, C.: Connecting large-scale atmospheric circulation,  
646 river flow and groundwater levels in a chalk catchment in southern England. *Journal of*  
647 *Hydrology*, 523, 179–189. <http://dx.doi.org/10.1016/j.jhydrol.2015.01.060>, 2015.



648

649 Lavers, D.A., Prudhomme, C., and Hannah, D.M.: Large-scale climate, precipitation and  
650 British river flows: Identifying hydroclimatological connections and dynamics. *Journal of*  
651 *Hydrology*, 395 (3–4), 242–255. <https://doi.org/10.1016/j.jhydrol.2010.10.036>, 2010.

652

653 López-Parages, J., and Rodríguez-Fonseca, B.: Multidecadal modulation of El Niño influence  
654 on the Euro-Mediterranean rainfall. *Geophysical Research Letters*, 39:L02704,  
655 <https://doi.org/10.1029/2011GL050049>, 2012.

656 Masina M., and Lamberti A.: A nonstationary analysis for the Northern Adriatic extreme sea  
657 levels, *Journal of Geophysical Research*, 118, <https://doi.org/10.1002/jgrc.20313>, 2013.

658 Massei, N., Durand, A., Deloffre, J., Dupont, J., Valdes, D., and Laignel, B.: Investigating  
659 possible links between the North Atlantic Oscillation and rainfall variability in northwestern  
660 France over the past 35 years. *Journal of Geophysical Research - Atmosphere*, 112, 1–10,  
661 <https://doi.org/10.1029/2005JD007000>, 2007.

662 Massei, N., Laignel, B., Deloffre, J., Mesquita, J., Moyelay, A., and Lafite, R., Durant, A.:  
663 Long-term hydrological changes of the Seine River flow [France] and their relation to the North  
664 Atlantic Oscillation over the period 1950–2008. *International Journal of Climatology*, 29,  
665 <https://doi.org/10.1002/joc.2022>, 2009.

666 Massei, N., Dieppois, B., Hannah, D. M., Lavers, D.A., Fossa, M., Laignel, B., and Debret, M.:  
667 Multi-time-scale hydroclimate dynamics of a regional watershed and links to large-scale  
668 atmospheric circulation: Application to the Seine river catchment, France. *Journal of*  
669 *Hydrology*, 546; 262–275, <https://doi.org/10.1016/j.jhydrol.2012.04.052>, 2017.

670 Menendez M., and Woodworth P. L.: Changes in extreme high-water levels based on a quasi-  
671 global tide-gauge data set, *Journal of Geophysical Research*, 115, C10011.  
672 <http://dx.doi.org/10.1029/2009JC005997>, 2010.



- 673 Milly, P.C.D, et al.: Stationarity is dead: whither water management? *Science* 319:573-574,  
674 2008.
- 675 Mizuta, R.: Intensification of extratropical cyclones associated with the polar jet change in the  
676 CMIP5 global warming projections. *Geophysical Research Letters*, 39, L19707, 1-6,  
677 <https://doi.org/10.1029/2012GL053032>, 2012.
- 678  
679 Nakamura, M., and Yamane, S.: Dominant anomaly patterns in the near-surface baroclinicity  
680 and accompanying anomalies in the atmosphere and oceans. Part I: North Atlantic basin.  
681 *Journal of Climate*, 22, 880–904. <https://doi.org/10.1175/2010JCLI3017.1>, 2009.
- 682  
683 Nakamura, H., Sampe, T., Goto, Ohfuchi, A. W., and Xie, S-P.: On the importance of  
684 midlatitude oceanic frontal zones for the mean state and dominant variability in the  
685 tropospheric circulation. *Geophysical Research Letters*, 35, L15709,  
686 <https://doi.org/10.1029/2008GL034010>, 2008.
- 687 Nicholls, R. J., Marinova, N., Lowe, J. A., Brown, S., Vellinga, P., De Gusmao, D., Hinkel, J.,  
688 and Tol, R. S.: Sea-level rise and its possible impacts given a “beyond 4 C world” in the twenty-  
689 first century, *Philosophical Transactions of the Royal Society A*, 369, 161–181.  
690 <https://doi.org/10.1098/rsta.2010.0291>, 2011.
- 691 Parey, S.: “Different ways to compute temperature return levels in the climate change context.  
692 *Environmetrics* , 21:698–718, 2010.
- 693 Philips, M. R., Rees, E. F., and Thomas, T.: winds, sea level and North Atlantic Oscillation  
694 (NAO) influences: An evaluation; *Global Planetary Change*, 100, 145-152,  
695 <http://dx.doi.org/10.1016/j.gloplacha.2012.10.01>, 2013.



- 696 Peings, Y., and Magnúsdóttir, G.: Forcing of the wintertime atmospheric circulation by the  
697 multidecadal fluctuations of the North Atlantic Ocean. *Environmental Research Letters*, 9  
698 (2014), 034018, 2014.
- 699 Pirazzoli, P.A.: A review of possible eustatic, isostatic and tectonic contributions in eight late-  
700 Holocene relative sea-level histories from the Mediterranean area. *Quaternary Science Review*,  
701 24 (18-19), 1989-2001 , <https://doi.org/10.1016/j.quascirev.2004.06.026>, 2005.
- 702 Rosbjerg, R. and Madsen, H.: Design with uncertain design values, *Hydrology in a Changing*  
703 *Environment*”, Wiley, 155–163, 1998.
- 704 Salas, J.D., and Obeysekera, J.: Revisiting the concepts of return period and risk for  
705 nonstationary hydrologic extreme events. *Journal of Hydrologic Engineering*,  
706 doi:10.1061/(ASCE)HE.1943-5584.0000820, 2013.
- 707 Sang, Y.F.: A review on the applications of wavelet transform in hydrology time series  
708 analysis. *Atmospheric Research* 122, 8–15. <http://dx.doi.org/10.1016/j.atmosres.2012.11.003>,  
709 2013.
- 710 Sutton, R.S., and Dong, B.: Atlantic Ocean influence on a shift in European climate in the  
711 1990s. *Nature Geosciences*, 5, 788–792, 2012.
- 712 Seager, R., Harnik, N., Kushnir, Y., Robinson, W., and Miller, J.: Mechanisms of hemispherically  
713 symmetric climate variability. *Journal of Climate*, 16, 2960–2978, 2003.
- 714 Tyrallis, H., Papacharalampous, G., and Tantane, S.: How to explain and predict the shape  
715 parameter of the generalized extreme value distribution of streamflow extremes using a big  
716 dataset. *Journal of Hydrology* 574:628–645. doi:10.1016/j.jhydrol.2019.04.070, 2019.
- 717
- 718 Tomasin A., and Pirazzoli P.A. : Extreme Sea Levels in the English Channel: Calibration of  
719 the Joint Probability Method. *Journal of Coastal Research* 24 4C 1-13 West Palm Beach,  
720 Florida July 2008, <https://doi.org/10.2112/07-0826.1>, 2008.



721 Torrence, C., and Compo, G.P.: A practical guide to wavelet analysis. B. American  
722 Meteorological Society, 79, 61–78. [http://dx.doi.org/10.1175/1520-0477\(1998\);](http://dx.doi.org/10.1175/1520-0477(1998);)  
723 079<0061:APGTWA>2.0.CO;2, 1998.

724 Trigo, R. M., Osborn, T. J., and Corte-Real, J.: The North Atlantic Oscillation influence on  
725 Europe: climate impacts and associated physical mechanisms. *Climate Research*, 20, 9–17.  
726 10.3354/cr020009, 2002.

727 Trisimplis, M. N., and Josey, S. A.: Forcing of the Mediterranean Sea by atmospheric  
728 oscillations over the North Atlantic. *Geophysical Research Letters*, 28, 803-806, 2001.

729 Turki, I., Laignel, B., Kakeh, N., Chevalier, L., and Costa, S., 2015a. Methodology for Filling  
730 gaps and Forecast in sea level: application to the eastern English Channel and the North  
731 Atlantic Sea (western France), *Ocean Dynamics*, <https://doi.org/10.1007/s10236-015-0824-z>,  
732 2015a.

733 Turki, I., Laignel, B., Chevalier, L., Massei, N., and Costa, S.: On the Investigation of the Sea  
734 Level Variability in Coastal Zones using SWOT Satellite Mission: example of the Eastern  
735 English Channel (Western France). *IEEE Journal of Selected Topic in Applied Earth*  
736 *Observations and Remote Sensing*, <http://dx.doi.org/10.1109/JSTARS.2015.2419693>, 2015b.

737 Turki, I., Massei, N., and Laignel, B.: Linking Sea Level Dynamic and Exceptional Events to  
738 Large-scale Atmospheric Circulation Variability: Case of Seine Bay, France. *Oceanologia*, 61  
739 (3), 321-330, <https://doi.org/10.1016/j.oceano.2019.01.003>, 2019.

740 Turki, I., Massei, N., Laignel, B., and Shafiei, H.: Effects of global climate oscillations in the  
741 intermonthly to the interannual variability of sea levels along the English Channel Coasts (NW  
742 France). *Oceanologia* (2020) 000, 1-17, <https://doi.org/10.1016/j.oceano.2020.01.001>, 2020.

743 Vousdoukas, M. I., Mentaschi, L., Voukouvalas, E., Verlaan, M., and Feyen, L.: Extreme sea  
744 levels on the rise along Europe's coasts. *Earth's Future*, 5, 504-323,  
745 <https://doi.org/10.1002/2016EF000505>, 2017.





746 Zampieri, M., Scoccimarro, E., and Gualdi, S.: Atlantic influence on spring snowfall over the  
747 Alps in the past 150 years. *Environmental Research Letters*, 8 (034026), 2013.

748 Zampieri, M., Toreti, A., Schindler, A., Escoccimarro, E., and Gualdi, S.: Atlantic multi-  
749 decadal oscillation influence on weather regimes over Europe and the Mediterranean in spring  
750 and summer. *Global and Planetary Change* 151, 92-100,  
751 <https://doi.org/10.1016/j.gloplacha.2016.08.014>, 2017.

752

753 Zappa, G., Shaffrey, L. C., Hodges, K. I., Sansom, P., and Stephenson, D. B.: A multimodel  
754 assessment of future projections of North Atlantic and European cyclones in the CMIP5 climate  
755 models. *Journal of Climate*, 26, 5846-5862, <https://doi.org/10.1175/JCLI-D-12-00573.1>, 2013.

756 Zhang, R., Delworth, T.L., Sutton, R., Hodson, D.L.R., Dixon, K.W., Held, I.M., Kushnir, Y.,  
757 Marshall, J., Ming, Y., Msadek, R., Robson, J., Rosati, A.J., Ting, M.F., and Vecchi, G.A.:  
758 Have aerosols caused the observed Atlantic multidecadal variability? *Journal of Atmospheric*  
759 *Sciences*, 70, 1135–1144, 2013.

760

761

762

763

764

765

766

767

768

769

770



771

772 *Table 1. The explained variance expressed as percentage of total variance of monthly extreme surges*  
 773 *for all sites.*

774

	~ 1.5-yr	~ 2-4-yr	~ 5-8-yr	~ 12-16-yr
<b>Brest</b>	<b>12.5%</b>	<b>7.5%</b>	<b>4.5%</b>	<b>1.9%</b>
<b>Cherbourg</b>	<b>14.8%</b>	<b>8.7%</b>	<b>5.2%</b>	<b>2.7%</b>
<b>Dunkirk</b>	<b>15.2%</b>	<b>8.6%</b>	<b>5.6%</b>	<b>3.2%</b>
<b>Dover</b>	<b>16.7%</b>	<b>9.9%</b>	<b>6.2%</b>	<b>3.9 %</b>
<b>Weymouth</b>	<b>16.5%</b>	<b>10.2%</b>	<b>7.9%</b>	

775

776

777

778

779

780 *Table 2. The mean explained variance expressed as percentage of total variance provided by the*  
 781 *wavelet coherence between the extreme surges and the climate Oscillations (SLP, ZW, NAO, AMO)*

782

783

784

	~ 1.5-yr	~ 2-4-yr	~ 5-8-yr	~ 12-16-yr
<b>SLP</b>	<b>75%</b>	<b>12%</b>	<b>15%</b>	<b>8%</b>
<b>ZW</b>	<b>10%</b>	<b>65%</b>	<b>12%</b>	<b>2%</b>
<b>NAO</b>	<b>6%</b>	<b>5%</b>	<b>60%</b>	<b>10%</b>
<b>AMO</b>	<b>0.2%</b>	<b>0.1%</b>	<b>1%</b>	<b>80 %</b>

785

786

787

788

789

790

791

792

793

794

795



796

797

798 *Table 3 AIC test results for the distribution models of the extreme surges using the stationary*  
 799 *(GEV0) and the nonstationary (GEV1-3) models combined with climate oscillations indices. The*  
 800 *stationary (GEV0) and nonstationary GEV (GEV1, GEV2 and GEV3) models are illustrated for each*  
 801 *time scale and each site. The lowest AIC values for each case are marked by grey colour.*

802

803

---

	~ 1.5-yr	GEV0	GEV1	GEV2	GEV3
	<b>Brest</b>	-2997	-3009	-3015	-3050
	<b>Cherbourg</b>	-1591	-1620	-1622	-1662
	<b>Dunkirk</b>	-1406	-1410	-1415	-1430
	<b>Dover</b>	-2186	-2190	-2195	-2200
804	<b>Weymouth</b>	-2180	-2192	-2198	-2214

805

¶

~ 2-4-yr

	<b>Brest</b>	-3015	-3018	-3025	-3020
	<b>Cherbourg</b>	-1511	-1620	-1642	-1622
	<b>Dunkirk</b>	-1414	-1417	-1434	-1420
	<b>Dover</b>	-2180	-2183	-2195	-2187
806	<b>Weymouth</b>	-2179	-2181	-2220	-2211

807

~ 5-8-yr

	<b>Brest</b>	-1962	-1980	-1922	-1940
	<b>Cherbourg</b>	-1827	-1937	-1878	-1870
	<b>Dunkirk</b>	-1797	-1850	-1815	-1810
	<b>Dover</b>	-2175	-2198	-2168	-2160
808	<b>Weymouth</b>	-2171	-2180	-2162	-2158

809

~ 12-16-yr

	<b>Brest</b>	-1258	-1980	-1922	-1940
	<b>Cherbourg</b>	-1225	-1212	-1205	-1198
	<b>Dunkirk</b>	-1398	-1381	-1367	-1351
	<b>Dover</b>	-1377	-1363	-1360	-1343
	<b>Weymouth</b>				

810

811

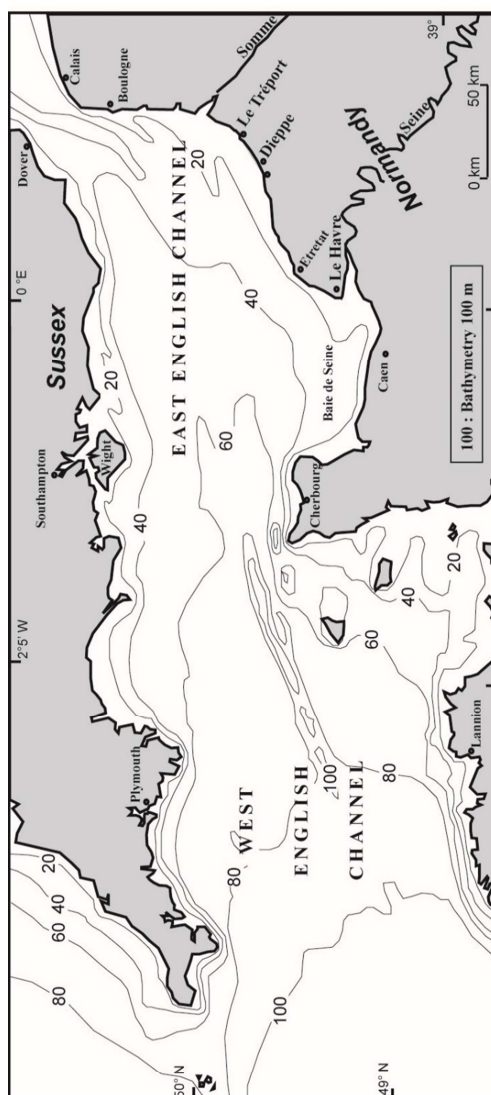
812

813



814 *Figure 1 Geographical location of the study area and the different tide gauges along the English*  
815 *Channel coasts: Brest, Cherbourg, Dunkirk (NW France); Dover and Weymouth (SW UK); (Figure*  
816 *extracted from Remi et al., (2010) modified).*

817



818

819

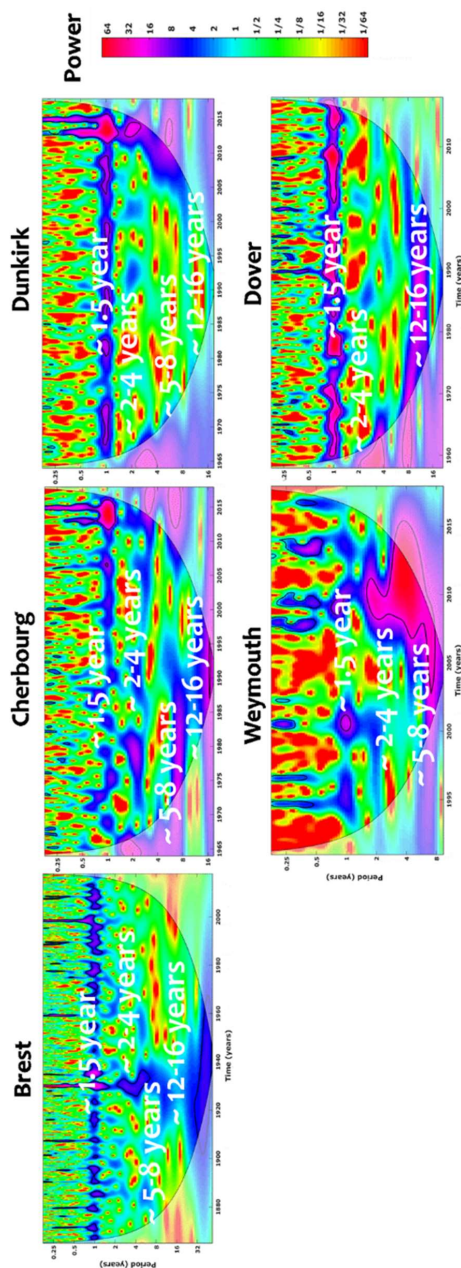
820

821



822 *Figure 2. CWT of monthly maxima of surges in Brest, Cherbourg, Dunkirk, Dover and*

823 *Weymouth.*



824

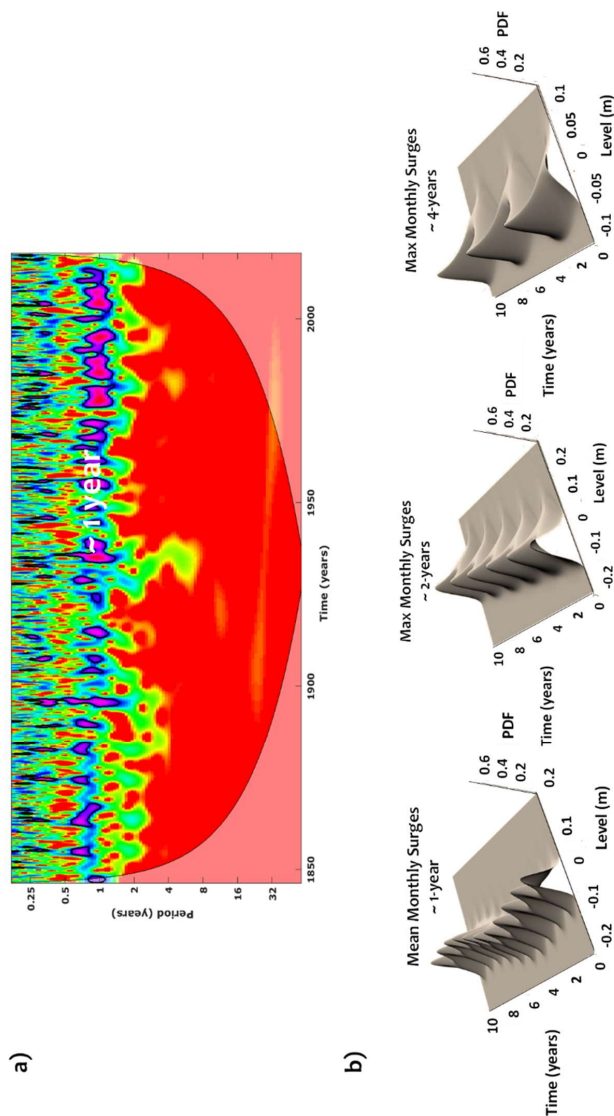
825



826

827 *Figure 3. Multiscale variability of the monthly mean and maximum surges in Brest. (a) CWT*  
828 *of monthly mean surges; (b) Interannual variability of monthly and extreme surges*

829



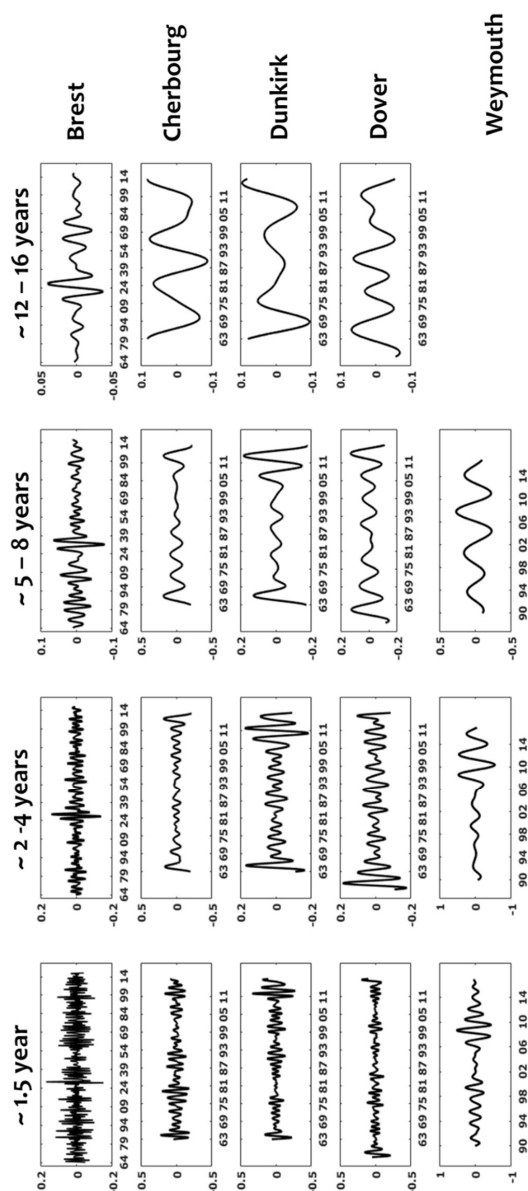
830

831

832



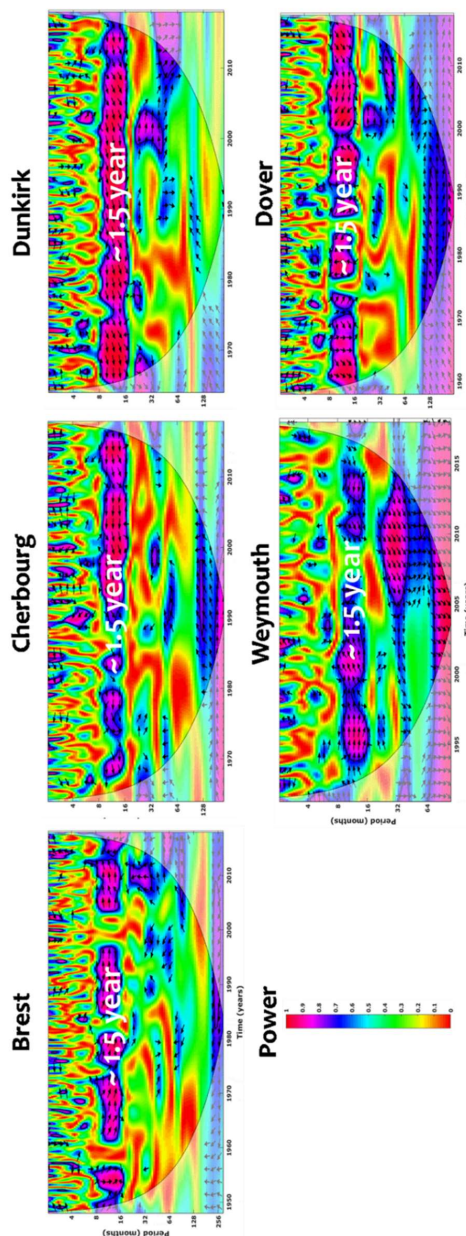
833 *Figure 4 Wavelet components resulting from the multiresolution analysis of surges at the*  
834 *interannual (~1.5-yr, ~2-4-yr and ~5-8-yr) and interdecadal (~12-16-yr) time scales for all*  
835 *sites (Brest, Cherbourg, Dunkirk, Dover and Weymouth).*  
836



837



838 *Figure 5. Wavelet Coherence (CW) between monthly extrema of surges and Sea Level*  
839 *Pressure (SLP).*

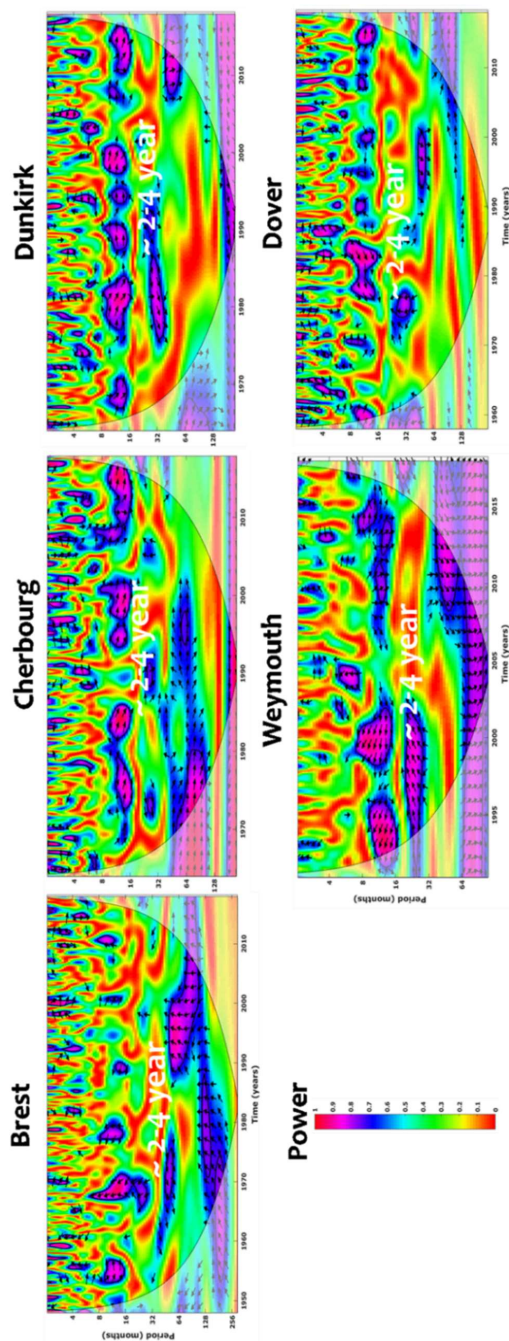


840





841 *Figure 6. Wavelet Coherence (CW) between monthly extrema of surges and Zonal Wind*  
842 *(ZW).*



843



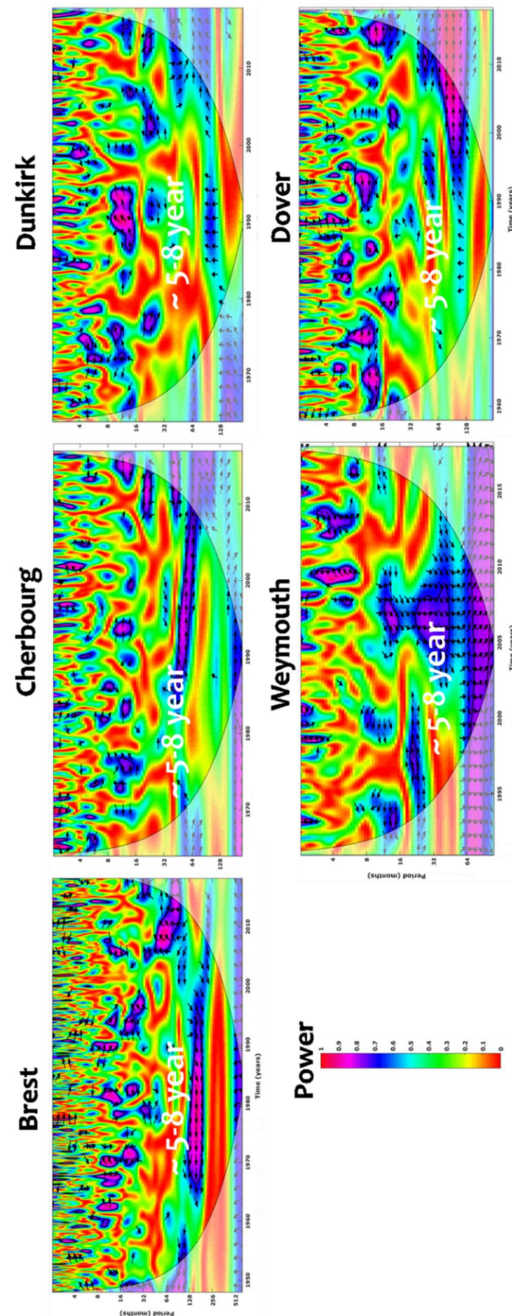
844

845

846 *Figure 7. Wavelet Coherence (CW) between monthly extrema of surges and North Atlantic*

847

*Oscillation (NAO).*

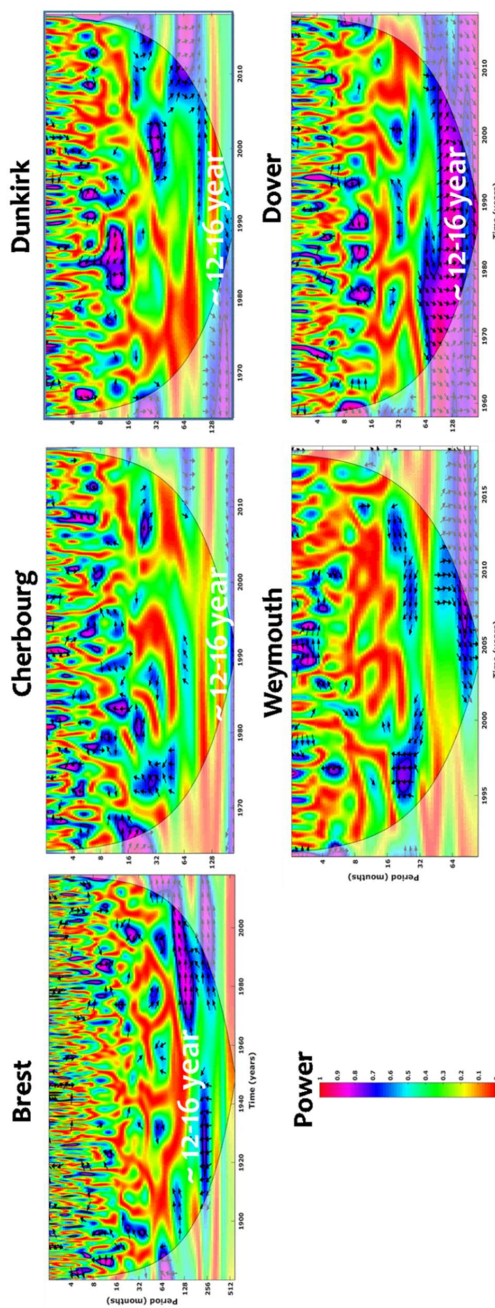


848

849

850

Figure 8. Wavelet Coherence (CW) between monthly extrema of surges and Atlantic  
Multidecadal Oscillation (AMO).



851  
852  
853  
854  
855



856

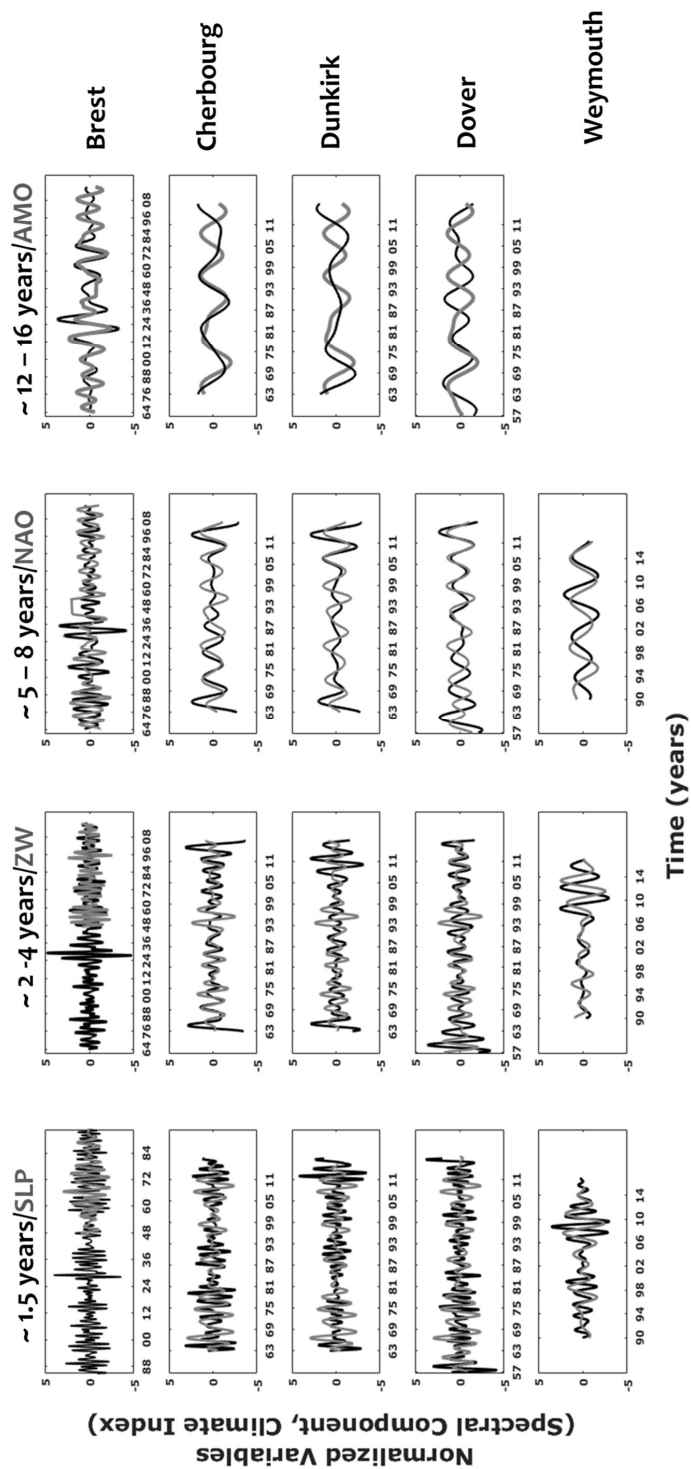
857

858

859 *Figure 9 Wavelet Components of monthly extreme surges (black lines), at the interannual (~ 1.5-yr ,*  
860 *~2-4-yr and ~5-8-yr) and interdecadal (~12-16-yr) time scales for all sites (Brest, Cherbourg, Dunkirk,*  
861 *Dover and Weymouth), correlated to the spectral component of climate oscillations associated to the*  
862 *different indices SLP, ZW, NAO and AMO (grey line). Only the connection maximizing the correlation*  
863 *coefficient between a selected climate index and the component of surges (from interannual to the*  
864 *interdecadal timescales) is presented (the normalized values have been calculated to superpose both*  
865 *signals).*

866

867



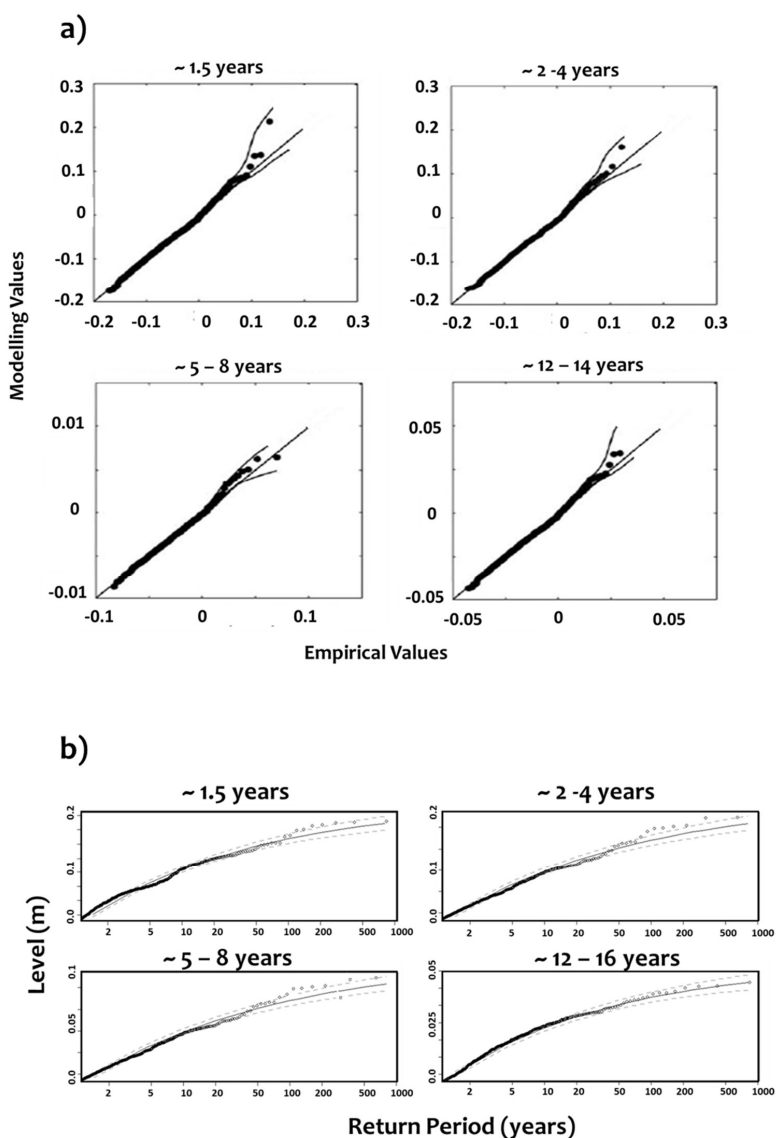


869

870 *Figure 10. a. The quantile plot between observed and modelled extreme surges by the use of the best*  
871 *GEV models, at different time scales, case of Brest. b. The Return level of extreme surges estimated*  
872 *for Brest using the best GEV models. The 95% confidence interval is presented with the dashed black*  
873 *line.*

874

875



876

877